8-2000

ROSAT HRI AND ASCA Observations of the Spiral Galaxy NGC 6946 and Its Northeast Complex of Luminous Supernova Remnants

Eric M. Schlegel
Smithsonian Astrophysical Observatory

William P. Blair
Johns Hopkins University

Robert A. Fesen
Dartmouth College

ROSAT HRI AND ASCA OBSERVATIONS OF THE SPIRAL GALAXY NGC 6946 AND ITS NORTHEAST COMPLEX OF LUMINOUS SUPERNOVA REMNANTS

ERIC M. SCHLEGEL,[1] WILLIAM P. BLAIR,[2] AND ROBERT A. FESEN[3]

ABSTRACT

Analysis of 80 ks *ASCA* and 60 ks *ROSAT* HRI observations of the face-on spiral galaxy NGC 6946 are presented. The *ASCA* image is the first observation of this galaxy above ~ 2 keV. Diffuse emission may be present in the inner $\sim 4'$ extending to energies above ~ 2–3 keV. In the HRI data, 14 pointlike sources are detected, the brightest two being a source very close to the nucleus and a source to the northeast that corresponds to a luminous complex of interacting supernova remnants (SNRs). We detect a point source that lies $\sim 30''$ west of the SNR complex but with a luminosity $\sim 1/15$ of the SNR complex. None of the point sources show evidence of strong variability; weak variability would escape our detection.

The *ASCA* spectrum of the SNR complex shows evidence for an emission line at ~ 0.9 keV that could be either Ne IX at ~ 0.915 keV or a blend of ion stages of Fe L-shell emission if the continuum is fitted with a power law. However, a two-component, Raymond-Smith thermal spectrum with no lines gives an equally valid continuum fit and may be more physically plausible given the observed spectrum below 3 keV. Adopting this latter model, we derive a density for the SNR complex of 10–35 cm^{-3}, consistent with estimates inferred from optical emission-line ratios. The complex's extraordinary X-ray luminosity may be related more to the high density of the surrounding medium than to a small but intense interaction region where two of the complex's SNRs are apparently colliding.

Key words: galaxies: individual (NGC 6946) — galaxies: spiral — supernova remnants — X-rays

1. INTRODUCTION

The first step in the study of the X-ray emission from spiral galaxies is the identification and characterization of a galaxy's point and extended sources, followed by a comparison of these source types across a broad range of galaxy properties. Prior to the launch of *ROSAT* in 1990, X-ray observations of spiral galaxies were limited to Local Group members or a few bright and relatively nearby galaxies such as M51, M81, and M83 (e.g., Fabbiano 1994 and references therein). *ROSAT* greatly expanded the number of galaxies for which more detailed observations could be undertaken owing in part to a sharper point-spread function and a lower detector background (Pfeffermann et al. 1986).

X-ray emission from the face-on, nearby, spiral galaxy NGC 6946 ($d = 5.1$ Mpc, de Vaucouleurs 1979; $N_H \sim 2$–3 $\times 10^{21}$ cm^{-2}, Burstein & Heiles 1984) was first observed with *Einstein* (Fabbiano & Trinchieri 1987). However, the relatively low spatial resolution of the data was insufficient to permit individual source identifications. More recent *ROSAT* PSPC observations detected about 10 sources (Schlegel 1994a), two of which have been identified as counterparts to optically detected supernova remnants (SNRs) (Schlegel 1994b; Blair & Fesen 1994; Van Dyk et al. 1994; Matonick & Fesen 1997). One of these is of particular interest owing to its unusually high optical and X-ray luminosity ($\sim 10^{40}$ ergs s^{-1} in the 0.2–2.0 keV band). Despite unusually high optical, radio, and X-ray luminosities suggestive of a young SNR, optical spectral data showed only relatively low expansion velocities. A *Hubble Space*

Telescope (*HST*) observation of this source has revealed that it is actually a complex of two or more unusually luminous remnants with an especially bright region marking an apparently strong collision between two of the remnants (Blair, Fesen, & Schlegel 2000, hereafter BFS00). The NGC 6946 SNR complex may be a younger example of the double SNR DEM L316 in the LMC (Williams et al. 1997). Dunne, Gruendl, & Chu (2000) present an alternative interpretation, describing MF 16 as the interaction of a strong wind with a nitrogen-rich circumstellar medium.

In addition to the X-ray point sources, unresolved emission was also detected across much of the galaxy in the PSPC data (Schlegel 1994a). This emission was interpreted as arising from a diffuse component likely representing emission from the galaxy's hot interstellar medium.

In this paper, we present both the *ROSAT* HRI image and an *ASCA* CCD observation (Tanaka, Inoue, & Holt 1994) of NGC 6946. These data consist of images of the galaxy and a spectrum of the extraordinary SNR, hereafter called MF 16 (the 16th entry on the SNR list of Matonick & Fesen 1997).

2. OBSERVATIONS

2.1. ROSAT HRI and PSPC

The *ROSAT* HRI was used to observe NGC 6946 for 60.3 ks spread across 15 days in 1994 May (Table 1). We used the HRI analysis software assembled by S. Snowden (Snowden 1998) to remove the particle background from the data, leaving 59.6 ks of deadtime-corrected exposure. Figure 1 shows the results after filtering and smoothing with an pyramid-shaped, adaptive filter (Lorenz et al. 1993) of 10 counts. The 10 count criterion represents a compromise between the preservation of spatial resolution and accumulating a high signal-to-noise ratio across the entire image. The HRI data have been overlaid onto an optical image from the digitized Palomar Sky Survey in Figure 2.

[1] Smithsonian Astrophysical Observatory, 60 Garden Street, Cambridge, MA 02138.

[2] Department of Physics and Astronomy, Johns Hopkins University, 3400 North Charles Street, Baltimore, MD 21218.

[3] Department of Physics and Astronomy, Dartmouth College, 6127 Wilder Lab, Hanover, NH 03755.

TABLE 1

OBSERVATION SUMMARY

Satellite	Instruments	Dates	JD	Exposure Time (ks)	Sequence
ROSAT	PSPC	1992 Jun 16–21	2,448,789–2,448,794	36.7	rp600272
ROSAT	HRI	1994 May 14–29	2,449,486–2,449,501	60.3	rh600501n00
ASCA	SIS, GIS	1994 Dec 28–1995 Jan 2	2,449,714–2,449,719	83.7	53040000

Point sources were detected using the *Chandra Observatory*'s *wavdetect* program, based on the wavelet code of Micela et al. (1996). We used a detection criterion of 1.0×10^{-6}, which permits at most approximately one false source. Point sources have been labeled and correspond to the entries in Table 2. The luminosities in Table 2 are tabulated for the 0.5–2.0 keV band assuming a 1 keV thermal bremsstrahlung spectrum absorbed by a Galactic column $N_{\rm H}$ of 2.5×10^{21} cm^{-2}. The luminosities differ from the adopted model by $\sim 25\%$ if the adopted model temperature is instead set to 5–7 keV.

Since the *ROSAT* PSPC data were published (Schlegel 1994a), several improvements in the pipeline processing have been made, particularly in the corrections for the bore-sight and aspect (Briel et al. 1996).[4] The data were obtained in 1992 June (Table 1). The reprocessed data were filtered using the diffuse analysis procedures available from the *ROSAT* data center and described by Snowden (1995).[5] After screening the data for particle background and solar-scattered X-rays, a total of 34.3 ks remained. The filtered PSPC image does not differ in any systematic way from that presented in Schlegel (1994a), so we do not include it to conserve space.

[4] Available by anonymous FTP to lheavx.gsfc.nasa.gov.
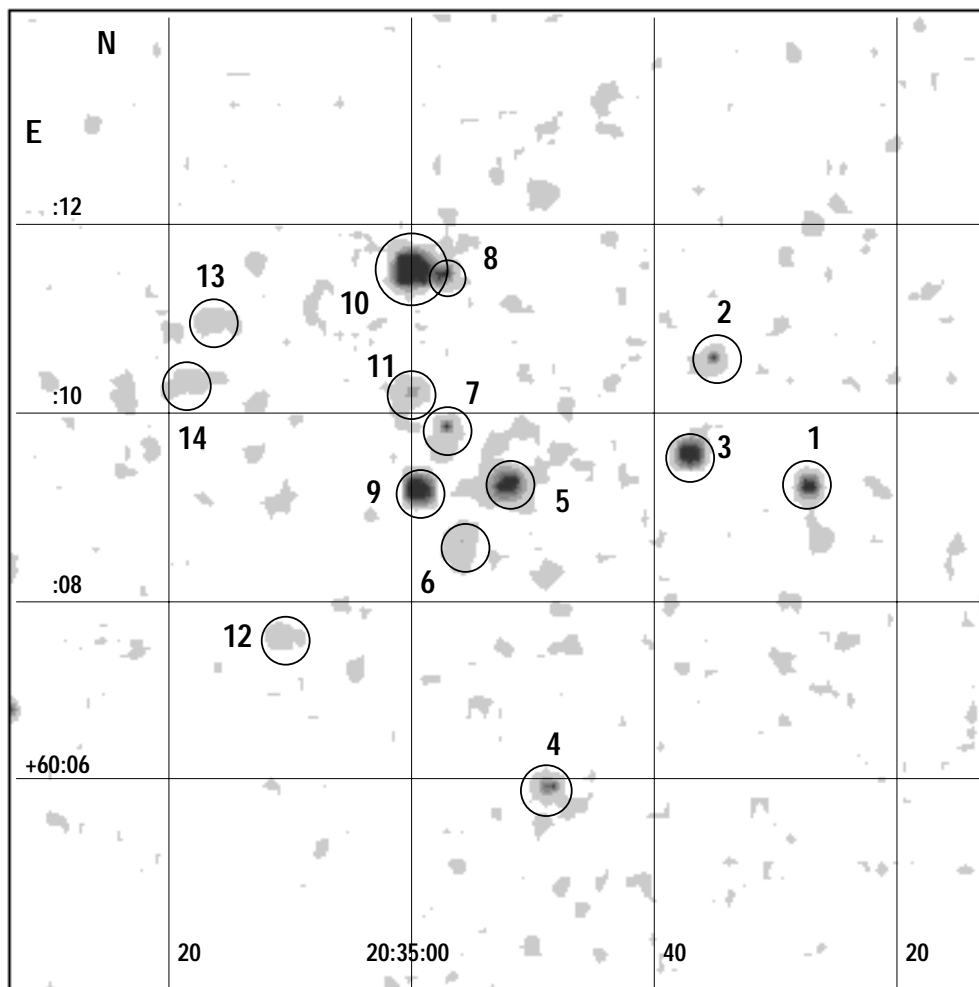[5] Available by anonymous FTP to legacy.gsfc.nasa.gov.

FIG. 1.—*ROSAT* HRI image of NGC 6946. North is up, and east is left. The panel is 8′ on a side. The data have been screened and adaptively smoothed using a smoothing scale of 10 counts. The point sources from Table 2 are identified.
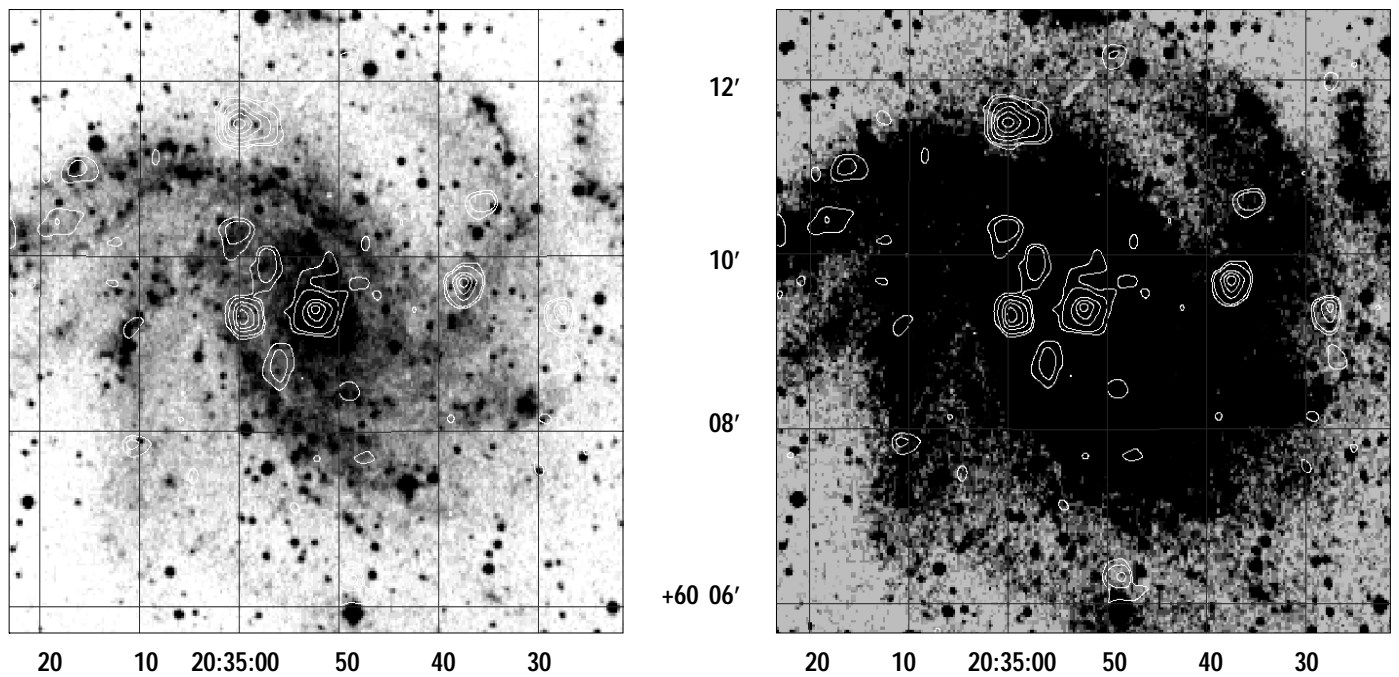
FIG. 2.—HRI image, contoured, on top of a digitized POSS image of NGC 6946. The images are 8′ on a side with north up and east left. The figures show the upper (*left*) and lower (*right*) ranges of the image scaling.

2.2. ASCA

The *ASCA* data were obtained from 1994 December 28 to 1995 January 2 for a total exposure time of 92 ks (Table 1). After applying the standard screening 83 ks of observation remained. The majority of the data ($\sim 75\%$) were obtained in 1-CCD mode with the remainder taken in 2-CCD mode. Data screening was applied to each data mode separately, and the results were registered and summed. The data were divided by energy into the following seven bands: 0.5–1.0, 1.0–1.5, 1.5–2.5, 2.5–3.5, 3.5–4.5, 4.5–6.5, and 6.5–9.5 keV. The corners of each image were used to define the background level which was then subtracted.

The point-spread function (PSF) of the *ASCA* mirrors has a FWHM of $\sim 3'$ and has a cross-shaped pattern (Tanaka et al. 1994). To recover the most information from

TABLE 2

ROSAT HRI Point Sources within 8″ of the Center of NGC 6946

Number	R.A. (J2000)[a]	Decl. (J2000)[a]	Counts ± Error	S/N	Rate[b]	Flux[c]	L_X[d]	Notes[e]
1	20 34 25.9	+60 09 05.4	64 ± 10.7	7.8	10.7 ± 1.8	2.8 ± 0.7	8.7 ± 2.1	x
2	20 34 34.5	+60 10 30.4	45 ± 10.4	4.7	5.9 ± 2.3	1.7 ± 0.6	5.3 ± 2.0	...
3	20 34 36.6	+60 09 29.9	138 ± 14.5	14.9	23.3 ± 2.4	6.6 ± 0.8	20.5 ± 2.5	x, o?, r
4	20 34 48.7	+60 05 48.5	42 ± 10.2	4.8	6.9 ± 2.3	2.3 ± 0.7	7.1 ± 2.0	x
5	20 34 52.4	+60 09 11.2	167 ± 18.7	11.5	27.9 ± 3.1	9.3 ± 0.9	28.8 ± 2.8	x, r?
6	20 34 56.8	+60 08 33.7	65 ± 14.6	4.8	10.9 ± 2.4	3.1 ± 0.7	9.6 ± 2.2	x, r
7	20 34 57.8	+60 09 47.3	57 ± 14.3	4.3	9.6 ± 2.4	2.7 ± 0.7	8.4 ± 2.1	...
8	20 35 00.6	+60 11 29.4	52 ± 10.1	4.2	8.7 ± 1.7	2.5 ± 0.5	7.8 ± 1.5	...
9	20 35 00.3	+60 09 05.8	196 ± 15.9	20.3	31.1 ± 2.6	9.7 ± 0.9	30.0 ± 2.8	x
10	20 35 00.7	+60 11 29.4	827 ± 31.4	61.3	138.2 ± 5.2	38.2 ± 1.4	118.4 ± 4.5	x, o, r
11	20 35 01.5	+60 10 04.4	45 ± 11.3	4.4	7.6 ± 1.9	2.8 ± 0.7	8.7 ± 2.1	x
12	20 35 11.7	+60 07 30.0	34 ± 9.6	4.0	5.7 ± 1.6	1.5 ± 0.6	4.6 ± 1.9	...
13	20 35 18.0	+60 10 54.1	41 ± 10.2	4.5	6.9 ± 1.7	1.7 ± 0.6	6.3 ± 2.4	...
14	20 35 20.7	+60 10 16.6	52 ± 12.1	4.1	8.7 ± 2.4	2.5 ± 0.7	7.8 ± 2.1	...

[a] Units of right ascension are hours, minutes, and seconds, and units of declination are degrees, arcminutes, and arcseconds. Positions accurate to $\sim \pm 1''$.

[b] Units: 10^{-4} counts s^{-1}.

[c] Flux, in units of 10^{-14} ergs s^{-1} cm^{-2}, calculated by adopting a 1 keV thermal bremsstrahlung spectrum absorbed by a column of 2.5×10^{21} cm^{-2}, so 1 count s$^{-1} \sim 2.8 \times 10^{-10}$ ergs s^{-1} cm^{-2} in the 0.5–2.0 keV band.

[d] Units: 10^{37} ergs s^{-1}.

[e] Notes.—The counterparts in other papers are indicated by a letter. Each letter is identified below. Question marks over an equals sign denote a possibly dubious identification. x = X-ray: PSPC data (Schlegel 1994a): 1 = PSPC-8; 3 = PSPC-2; 4 = PSPC-9; 5 = PSPC-3; 6 = PSPC-6; 9 = PSPC-4; 10 = PSPC-1; 11 = PSPC-7; sources 2, 7, 12, 13, and 14 are weak, but visible in the PSPC data; source 8 is unresolved in the PSPC data. r = Radio: Lacey et al. 1997 (LDG97): 3 = LDG97-22; 5 $\stackrel{?}{=}$ LDG97-56; 6 = LDG97-80; 10 = LDG97-85. o = optical: Matonick & Fesen 1997 (MF97): 10 = MF97-16; 3 $\stackrel{?}{=}$ MF97-4.
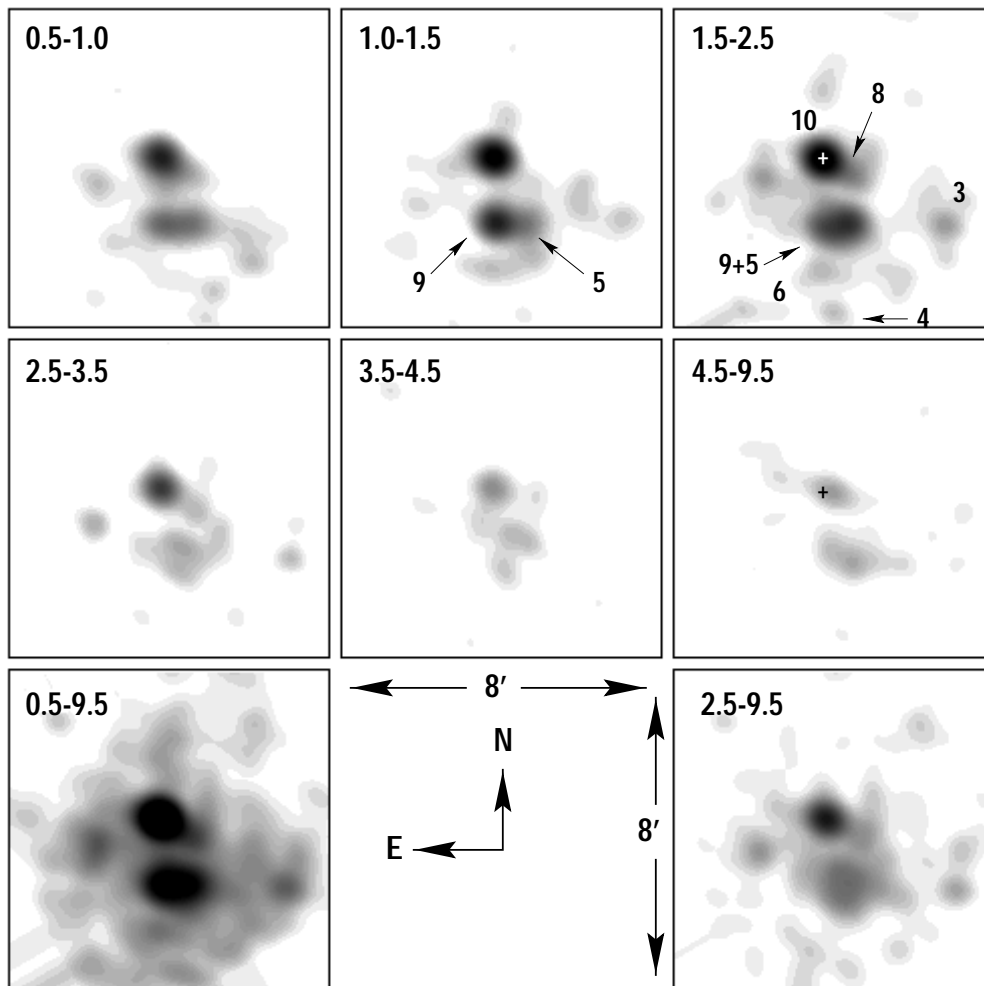
Fig. 3.—Montage of deconvolved *ASCA* images of NGC 6946. The energy band of the data in the individual panels increases to the right and to the bottom. The energies included in the panels are 0.5–1.0, 1.0–1.5, 1.5–2.5, 2.5–3.5, 3.5–4.5, and 4.5–9.5 keV. The bottom right-hand panel is the sum of all of the bands. North is up, and east is left. Each panel is 8′ on a side. The plus sign in the 1.5–2.5 and 4.5–9.5 panels indicates the centroid position of MF 16 from the 1.0–1.5 keV panel. Note how the centroid of emission shifts westward in the higher energy panel.

the image of NGC 6946, we deconvolved the PSF from the image using a point source filtered into the seven energy bands and the Lucy-Richardson deconvolution (the task as coded in the IRAF/STSDAS[6] " restore " package) following the prescription in Jalota, Gotthelf, & Zoonematkermani (1993). The noise in the corners of the image were monitored by calculating the rms average value after each iteration. The restoration was stopped when the rms value approached an asymptotic value (typically, ∼ 20 iterations).

The relatively high foreground column density to NGC 6946 nearly eliminates any photons below 0.5 keV, so we did not include any counts below that energy. Figure 3 shows a montage of the results; the energy band increases left to right, top to bottom.

As a test of the deconvolution, we blurred the *ROSAT* HRI data with the *ASCA* PSF. To obtain the PSF as a function of energy, we filtered the data of a point source (3C 273, sequence 70023000) into the seven *ASCA* energy bands

defined above. We then convolved those PSF bands with energies less than 2.5 keV with the HRI image and summed the results. We also filtered the raw *ASCA* counts to retain only those events with $E < 2.5$ keV. Figure 4 shows the summed image and the filtered raw *ASCA* data. Note the difference between the real (*lower right*) and the artificial (*upper right*) *ASCA* data. Figure 4 will be used below to help interpret the deconvolved *ASCA* data.

3. ANALYSIS AND DISCUSSION

3.1. *ROSAT HRI Data*

The *ROSAT* HRI image of NGC 6946 was used to inventory the galaxy's point sources. Since the *ROSAT* HRI offers little spectral resolution (Prestwich et al. 1997), we used a sliding box detection algorithm (box size 8″) to locate and to identify candidate point sources. Table 2 lists the sources detected and their count rates. HRI sources are designated with an " H " followed by a serial number. The counts were extracted using circular apertures 48″ in diameter. The background was determined from an aperture 5′ in diameter positioned well away from the galaxy and corrected for vignetting at that location.

The HRI image (Fig. 1) shows that many of the point sources identified in the PSPC data (Schlegel 1994a) are still
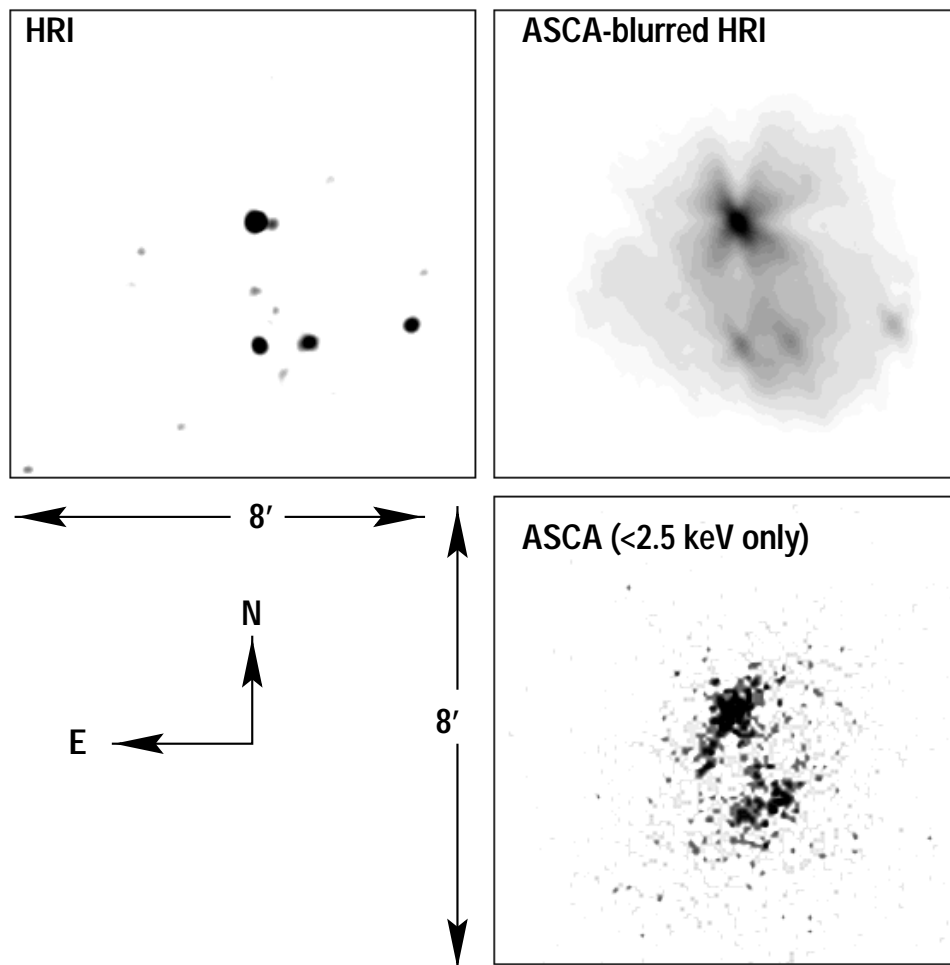
Fig. 4.—HRI image blurred with the *ASCA* PSF and compared directly to the background-subtracted *ASCA* image. The top left-hand panel shows the screened HRI data, extracted to match the centering and scale, but *not* the rotation angle, of the *ASCA* data. The top right-hand panel shows the HRI data blurred by the *ASCA* PSF for $E < 2.5$ keV. The bottom right-hand panel shows the *ASCA* SIS data filtered to include only events with $E < 2.5$ keV. Note the slight rotation of the *ASCA* image ($\sim 20°$, counterclockwise). North is up, and east is left. Each box is 8′ on a side.

present and remain at essentially identical relative intensities as in the PSPC data. In particular, HRI sources H1, H3, H5, H6, H9, H10 (SNR MF 16), and H11 are all clearly detected in the PSPC image. Table 2 lists the correspondences between the sources detected in the HRI data and those detected in the PSPC data. Spectral fits and hardness values from the PSPC data showed that all of the sources within 8′ of NGC 6946 were consistent with sources in NGC 6946 (or behind it) (Schlegel 1994a). Based on a Galactic log N–log S relation (Krautter et al. 1999), we expect ~ 0.1 stars to fall by chance within a radius of 5′ of NGC 6946. Using their extragalactic log N–log S (their active galactic nucleus ["AGN"] curve), we expect 0.04 AGNs within the same 5′ radius.

If we correct for the count rate differences between the PSPC and the HRI, all of the sources are consistent with a constant between the PSPC and HRI epochs. The large uncertainty in the conversion from PSPC to HRI counts prohibits a stronger statement. Within the HRI data, individual pointings are less than ~ 2 ks in length. Only the strongest sources (H5, H9, H10) were examined for variability, and none show evidence of variability greater than 90% confidence. The X-ray constancy of sources in NGC 6946 is in marked contrast to some other galaxies, for example,

NGC 1313, where about a half-dozen sources have been detected as variable objects (Schlegel et al. 2000). We turn now to a discussion of the individual sources.

The extraordinary X-ray luminosity of the MF 16 SNR complex is obvious in Figures 3, 4, and 5, where it is the dominant X-ray source in NGC 6946. Therefore its X-ray spectral properties are of special interest. The MF 16 complex and environs are resolved in the HRI data into two sources; MF 16 itself (H10) and a fainter additional source, H8, $\sim 30″$ farther to the west-southwest (see Fig. 1) with a luminosity $\simeq 6.5\%$ that of H10. H8 produces significant count contamination in the MF 16 spectrum in both the *ROSAT* PSPC and *ASCA* data, leading to uncertainty in the spectral behavior of MF 16.

Unfortunately, the nature of H8 is unknown. It is not directly attributable to an OB association that is near MF 16 (BFS00) because H8 lies $\sim 10″$ west of the association. The luminosity of H8 is $\sim 10^{38}$ ergs s^{-1} and thus not unlike that of X-ray binaries (White, Nagase, & Parmar 1995), suggesting one possible identification. Its contamination of H10 (MF 16) is particularly serious if H8 has a systematically different spectrum than the SNR complex. As an example, if MF 16 can be described by a Raymond-Smith plasma at 1 keV and the putative XRB by a thermal bremss-

trahlung component of 5 keV, as is typical of X-ray binaries, the merged spectrum will be increasingly dominated by the 5 keV bremsstrahlung emission above ~ 3 keV even with a 15:1 ratio in the total 0.5–2.0 keV luminosities. This will make the interpretation of the *ASCA* SIS data more difficult.

The source H5, although close to the center of NGC 6946, may not correspond to the X-ray emission from the galaxy's nucleus. The differences in the position of MF 16 between the HRI data and the VLA data (Van Dyk et al. 1994) amount to $\Delta\alpha = +0\rlap{.}{''}6$, $\Delta\delta = -1''$ (defined as HRI − VLA). Only one other source in the HRI field is positively identified: the Algol variable DT Cep, which lies 12′ off-axis. The differences between the optical and HRI positions are $\Delta\alpha = +6''$, $\Delta\delta = -9''$ (defined as HRI − optical) (Krautter et al. 1999). These differences are typical of the uncertainties of the *ROSAT* boresight offsets (Kürster & Hasinger 1993). If we use these MF 16 offsets to correct the position of H5, because they are nearly on-axis, the revised X-ray coordinates (Table 2) place it within 4″–5″ of the radio nucleus.[7] In the optical, the center of light, assumed to be the nucleus, appears to lie *south* of the position of the radio nucleus and H5 by $\sim 15''$–$20''$. The PSPC spectrum (Schlegel 1994a) of the "nuclear" source is soft with a fitted thermal bremsstrahlung temperature of ~ 0.5 keV. The source is consistent with the point-spread function of the HRI. The 0.5–2.0 keV luminosity is $\sim 3 \times 10^{38}$ ergs s^{-1}, which is highly sub-Eddington ($\sim 3 \times 10^{-7}$) if the nucleus were considered to be an accreting black hole of $\sim 10^7 M_\odot$ based on the black hole mass-bulge luminosity correlation (e.g., Kormendy & Richstone 1995) and the bulge luminosity of ~ -17.1 (Simien & de Vaucouleurs 1986; Kim & Chun 1984).

Recently, Colbert & Mushotzky (1999) have shown that a population of offset "nuclear" sources may exist at the center of galaxies. They found that, of those nearby ($v_{\rm red} < 1000$ km s^{-1}) galaxies for which X-ray observations exist, about half contain an X-ray source consistent with an off-center point source, each of which has a luminosity of $\sim 10^{39}$–10^{40} ergs s^{-1}. They suggest these sources are 10^2–$10^4 M_\odot$ black holes. NGC 6946 was one of the galaxies on their list of detections.

Four sources are detected in the HRI image that are weak but are visible in the PSPC data. These are H2, H12, H13, and H14. PSPC source 5, which lies $\sim 1\rlap{.}{'}5$ northwest of MF 16 and has an L_X of 5.5×10^{37} ergs s^{-1}, is not detected in the HRI observation. A drop even as small as ~ 30 in its luminosity would place the source below the HRI detection threshold. Source H7 was not resolved in the PSPC data. In that data set, it sits within the broad band of unresolved emission near the nucleus of NGC 6946.

In the HRI data, we detect none of the diffuse emission seen in the PSPC data, but we can easily understand why. The conversion factor of HRI counts to PSPC counts ranges from ~ 2.2 (Schlegel, Petre, & Colbert 1996) to ~ 2.8 (Zimmermann et al. 1994) depending upon the adopted spectral shape. We arbitrarily adopt a conversion of 2.5 HRI counts to 1.0 PSPC count so we can illustrate the limitations of the HRI for the detection of diffuse emission. To reach a sensitivity similar to that of the PSPC, the HRI

exposure time must be longer than the PSPC exposure time by at least the conversion factor. Strictly on the basis of the conversion factor, the 60 ks HRI exposure corresponds to an approximate PSPC exposure of 24 ks. This is substantially less than the actual duration of the PSPC observation in which the diffuse emission was detected (Schlegel 1994a). An alternative approach illustrates the same point. The PSPC-detected surface brightness is $\sim 5 \times 10^{36}$ ergs s^{-1} arcmin^{-2} (value from Schlegel 1994a corrected for arithmetic error). That brightness generates approximately 10^{-4} counts s^{-1} arcmin^{-2} in the PSPC while the internal PSPC background is $\sim 3 \times 10^{-5}$ counts s^{-1} arcmin^{-2} (Snowden et al. 1992), for a ratio of ~ 3. For the HRI, the same surface brightness produces $\sim 6 \times 10^{-6}$ counts s^{-1} arcmin^{-2} compared with the internal background of $\sim 4 \times 10^{-3}$ counts s^{-1} arcmin^{-2} for a ratio of ~ 0.002 (David et al. 1995).[8] The diffuse emission is overwhelmed by the internal background of the HRI.

3.2. *ASCA Data*

The deconvolved *ASCA* image of NGC 6946 is shown in Figure 3. This is the first image of NGC 6946 at energies above 2 keV. We filtered the *Einstein* IPC image into $E < 2$ keV and $E > 2$ keV; there are no photons above ~ 2 keV. The *ASCA* can be compared to the HRI image blurred with the *ASCA* PSF shown in Figure 4. Unlike the blurred HRI data, which contain no true diffuse emission, the *ASCA* image shows point sources that are embedded in diffuse emission. Below we will use the HRI image shown in Figure 4 to interpret the deconvolved *ASCA* data.

The bright point sources (H3, H5, H9, and H10) are deconvolved (although the deconvolution does not separate H5 and H9 except in the 1.0–1.5 keV panel where the counts are highest). Diffuse emission surrounds the nuclear sources, most visibly present in the 1–2 keV range (additional discussion follows below). There is also crude spectral information visible in the deconvolved figure for several of the point sources. Sources H3, H6, and H9 are weak above ~ 3 keV. For H5 and H9, the centroid of emission shifts from H9 to H5 between the 0.5–1.0 keV panel (*upper left*) and the 4.5–9.5 keV panel (*center row, right*), implying that $\sim 30\%$ of the flux of H5 lies above 3 keV. This behavior matches the spectral fit to the PSPC data of H5, which assigned only a lower limit to the temperature of $\gtrsim 0.5$ keV (Schlegel 1994a).

The deconvolved images also provide support for the identification of H8 as an X-ray binary. Even though the binary is blended with MF 16, the shape of the deconvolved image becomes an ellipse above ~ 5 keV, oriented east-west. We used the "ellipse" task in the STSDAS package to fit ellipses to the images in the 1.0–2.5 and 4.5–9.5 keV bands. The ellipticity in the higher energy panel is significant at the ~ 4 level, while the lower energy fits are consistent with zero ellipticity, both outward to an intensity level 70% below the maximum. That implies either that MF 16 is contributing a decreasing fraction of the flux of the total flux or that H8 contributes an increasing fraction. If H8's spectrum is typical of our Galaxy's population of low-mass XRBs, we expect to see a bremsstrahlung spectrum with $kT \sim 7$ keV in the *ASCA* band (e.g., White et al. 1995). For such a spectrum, normalized to the count rate in the HRI image, we estimate $\sim 60\%$ of the flux to lie above 3 keV and $\sim 25\%$

---

[7] The position of the radio nucleus is (J2000) α: $20^h34^m52\rlap{.}{^s}33$; δ: $+60°09'14\rlap{.}{''}23$ (Van Dyk et al. 1994).

[8] Available by anonymous FTP to lheavx.gsfc.nasa.gov.

above 6 keV. These estimates increase if H8 is more similar to a Galactic high-mass X-ray binary. The deconvolved *ASCA* image suggests H8 is not harder than $\sim$4–7 keV because otherwise we would see a definite point source in the hardest *ASCA* bands. An observation with higher spatial resolution and moderate to good spectral resolution is required to establish definitively the source type for H8.

Before leaving the discussion of the point-source population, we note the publication of a recent radio survey of NGC 6946 by Lacey, Duric, & Goss (1997). They used the VLA at 6 and 20 cm to carry out a search for compact radio sources. Source 85 on their list corresponds to the MF 16 SNR complex to within $\sim 0''.5$ verifying the identification of Van Dyk et al. (1994). The correspondence of other sources is included in the notes of Table 2 but can be summarized briefly. Each of the "strong" sources (those with S/N > 4.5) has a compact radio counterpart except H1 and H9.

Finally, there is apparent diffuse emission distributed across the face of the galaxy in the deconvolved images (Fig. 3). This emission was detected in the PSPC image (Schlegel 1994a). If the deconvolution process has recovered all of the photons of the point sources, then the spectrum of the diffuse component extends to energies of $\sim$3 keV. Support for the correctness of the deconvolution is the match in the overall appearance of Figure 3 to the PSPC image (Schlegel 1994a), where we know diffuse emission was detected. To examine the significance of the potential emission, we extracted all counts in an 8' radius circle encompassing the galaxy, excluding the counts within 2''.5 surrounding each of the point sources. The excluded zone leaves $\sim$30% of the flux of a point source outside of the aperture (Jalota et al. 1993). The counts in the galaxy aperture, in the 0.5–2.0 keV band in common with the PSPC, total $\sim 5 \times 10^{-5}$ counts s^{-1} arcmin^{-2}. The background is $\sim 2.0 \times 10^{-5}$ counts s^{-1} arcmin^{-2}. To this background value we must add the photons in the wings of the PSF. Sources 3, 5, 9, and 10 contribute more than 90% of the total counts in the 0.5–2.0 keV band. If we assume these counts raise the background uniformly, then an additional $\sim 2.2 \times 10^{-5}$ counts s^{-1} arcmin^{-2} exists. The ratio of the detected diffuse emission to the sum of the backgrounds is $\sim$1.2.

We set a limit on the luminosity of additional point sources of $\sim 5 \times 10^{37}$ ergs s^{-1}, about 25% lower than the limit from the PSPC data. Either the diffuse emission is truly diffuse or a gap exists, at about a few 10^{37} ergs s^{-1}, in the point-source luminosity function for this galaxy. The definitive properties of the diffuse emission must await

observations with the *Chandra X-Ray Observatory* or *XMM*.

3.3. *The MF 16 SNR Complex*

A sensitive search for emission lines from the hot gas in the spectrum of MF 16 constituted one of the prime purposes for the *ASCA* observation. We extracted the SIS source counts in a region 8' in radius. We only used the SIS data because of that instrument's superior spectral resolution. For the background, we extracted the counts from all pixels outside of the source aperture. We tested the background subtraction by extracting the counts from a "blank sky" observation[9] using the source aperture.

Extracted SIS data were then used to construct a model fit. Because the low-energy calibration of the SIS is inaccurate below $\sim$0.5 keV (Dotani et al. 1997) while the *ROSAT* PSPC is sensitive to the column density, $N_{\rm H}$, we combined the *ROSAT* PSPC and the SIS data. MF 16's evolution should be sufficiently slow that little spectral evolution will occur during the $\sim$2.5 yr gap between observations. The *ROSAT* PSPC spectrum was extracted using an aperture of 1'; the background was defined by an aperture 8' due west and well outside the galaxy's detected diffuse emission structure. We temporarily ignored data near the positions of expected lines (e.g., Fe Kα, Fe L, Si Kα) and used the remaining SIS + PSPC data to define the continuum. Once we had a successful continuum fit, we used all the data to search for emission lines in the SIS spectrum by adding one or more Gaussians to represent the line(s). The fit results are listed in Table 3.

The resulting continuum contours after fitting the PSPC + SIS spectrum with an absorbed power law are shown in Figure 5. From the dust maps of Schlegel, Finkbeiner, & Davis (1998), the value of E_{B-V} in the direction of NGC 6946 is 0.342. Using the column density–E_{B-V} relation of Predehl & Schmitt (1995), that value of E_{B-V} converts to $N_{\rm H} \sim 1.8 \times 10^{21}$ cm^{-2}. The column density derived from the model fit to the *ASCA* data is $\sim 2 \pm 0.2 \times 10^{21}$ cm^{-2}. The measured E_{B-V} toward the MF 16 complex is 0.65 (BFS00), which implies patchy extinction on an unresolved spatial scale. Very likely, the X-ray column is an "effective" column that arises from the area-weighted average of spatially variable extinction. As a test of our

---

[9] "Blank sky" observations are available from the *ASCA* GOF at NASA-GSFC.

TABLE 3

SUMMARY OF SPECTRAL FITTING[a] FOR THE SNR MF 16

Model	$N_{\rm H} \times 10^{21}$ cm^{-2}	First Parameter[b]	Second Parameter[b]	Mean SIS Norm	Ratio of Norms (1:2)	Overall χ^2/ν
Power Law	$1.88^{+0.32}_{-0.28}$	$2.34^{+0.14}_{-0.11}$	...	4.4(−4)	2.1	0.98
+ Gaussian...........		$0.90^{+0.05}_{-0.04}$	$0.10^{+0.05}_{-0.04}$	2.2(−4)	...	...
Brems-1	$4.96^{+0.42}_{-0.67}$	$0.22^{+0.04}_{-0.07}$	...	7.7(−2)	148	0.99
+ Brems-2		$3.0^{+0.7}_{-1.0}$	...	5.2(−4)	...	...
Raymond-1	$0.83^{+0.22}_{-0.14}$	$0.83^{+0.02}_{-0.08}$	1.0	1.0(−4)	0.14	1.01
+ Raymond-2........		$4.1^{+0.8}_{-0.2}$	1.0	7.2(−4)	...	...
Low-Z Ray-1	$0.99^{+0.14}_{-0.12}$	$0.86^{+0.05}_{-0.08}$	0.5	2.1(−4)	0.19	1.03
+ Low-Z Ray-2......		$3.2^{+0.9}_{-0.6}$	0.5	1.1(−3)	...	...

[a] All of the fits were carried out first using the PSPC + SIS data with regions near lines screened out of the fit and then searching for lines using the all the data.

[b] Parameters are defined as follows: Bremsstrahlung: first: temperature (keV), second: none; Gaussian: first: line position (keV), second: line width (keV); power law: first: power-law index, second: none; Raymond-Smith: first: temperature (keV), second: abundance (fixed during the fit)
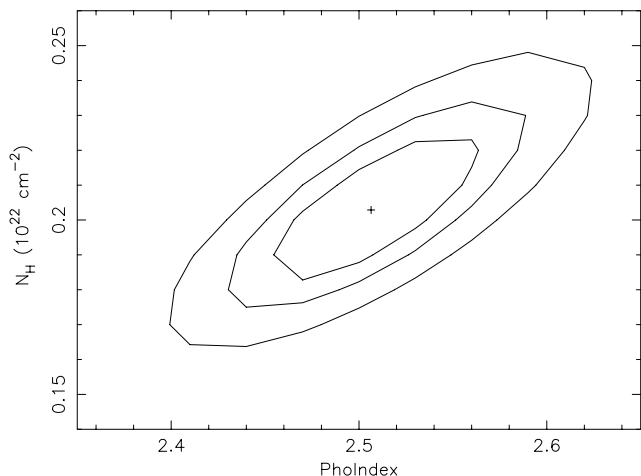
FIG. 5.—Contours on the fitted continuum parameters for the MF 16 region from the PSPC + GIS spectral data using a power law to fit the continuum.

FIG. 7.—Contours on the fitted emission line parameters from the PSPC + SIS fit using a power law for the continuum.

interpretation, when we fix the column at the BFS00 value, the resulting fit is very poor with $\Delta\chi^2/\nu \sim 1.5$.

The best single-component fit to the continuum yields a power-law index of ~ 2.5. The unavoidable presence of the neighboring source H8 in the combined spectrum may artificially lower the power-law index by inputting more energy above ~ 5 keV than the SNR alone. Nonetheless, from our fit we estimate an unabsorbed 0.5–2.0 keV luminosity of $\sim 2 \times 10^{40}$ ergs s^{-1} and the 2.0–10.0 keV luminosity of $\sim 7 \times 10^{39}$ ergs s^{-1}.

We see distinct residuals near 0.8–0.9 keV (Fig. 6). The apparent line that is best fitted by a width (σ) of ~ 0.1 keV is centered at 0.91 keV (Fig. 7). The equivalent width of the line is 157 ± 50 eV. If we interpret the line as a δ-function at the measured energy, it corresponds to Ne IX at either 0.915 or 0.922 keV. Conversely, the line might represent a blend of Fe L-shell emission from Fe XIX and Fe XX (Kallman et al. 1996). However, unless the Fe abundance is enhanced, high ionization stages of Fe L-shell emission are accompanied by Kα lines of medium-Z elements (e.g., Ne, Mg). Unfortunately, we have no information regarding the Fe abundance from the *ASCA* data. The poor signal-to-noise ratio

above ~ 5 keV places only a weak limit on the presence of an line in the 6.4–6.7 keV band (no line greater than 1 keV equivalent width), so we can not deduce any information about the presence of Fe L based on the presence or absence of Fe K.

Two alternative, equally valid fits use either dual bremsstrahlung or dual Raymond-Smith components. We followed the same fitting procedure (i.e., first PSPC + SIS continuum, then line search). In neither case do we detect emission lines in the model fits. The fitted bremsstrahlung temperatures are $0.21^{+0.02}_{-0.04}$ and $3.0^{+0.4}_{-0.6}$ keV, respectively. The fitted data, using the Raymond-Smith model, appears in Figure 8 and the parameter contours are shown in Figure 9. The fitted Raymond-Smith temperatures are $0.81^{+0.04}_{-0.05}$ keV and $4.2^{+0.6}_{-0.4}$ keV. The unabsorbed 0.5–2.0 keV luminosity is $\sim 9.6 \times 10^{39}$ ergs s^{-1} and the 2–10 keV luminosity is $\sim 1.1 \times 10^{40}$ ergs s^{-1}, which are about a factor of 2 lower and 1.6 higher, respectively, than the computed luminosities from the power-law model. The lower flux in the 0.5–2.0 keV band comes from the improved fit to the low-energy channels which reduces the column density.

Although the *ASCA* spectra do not have sufficient signal-to-noise ratio to constrain the abundance values, we can
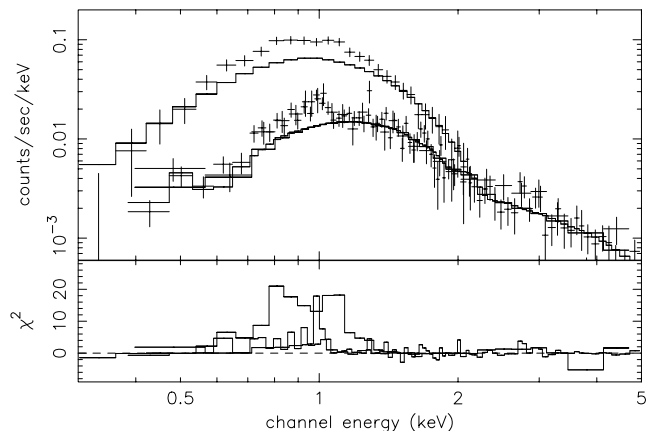

FIG. 6.—PSPC + SIS spectrum of the MF 16 region. For clarity, only the PSPC spectrum and one SIS spectrum are shown (*top*). The normalization of the line model has been set to zero to enhance its visibility. The continua were fitted using a power law. *Bottom*: The contributions to the remaining χ^2 of the fit.
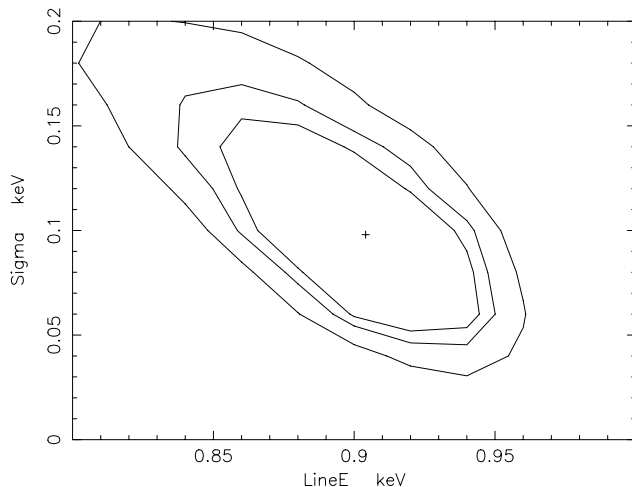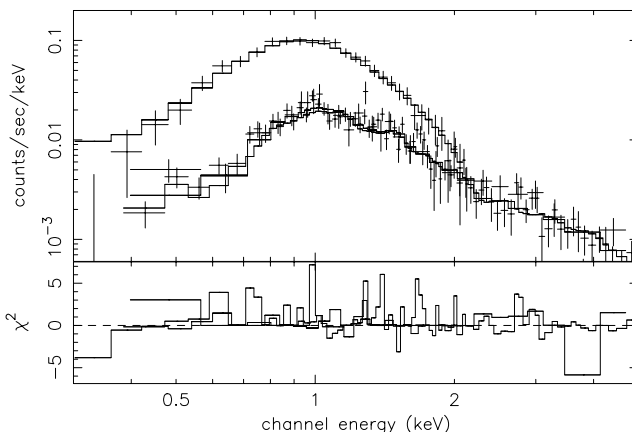

FIG. 8.—Spectral fit using the dual Raymond-Smith model. Only the PSPC spectrum and one SIS spectrum are plotted for clarity (*top*). *Bottom*: The contributions to the remaining χ^2 of the fit.
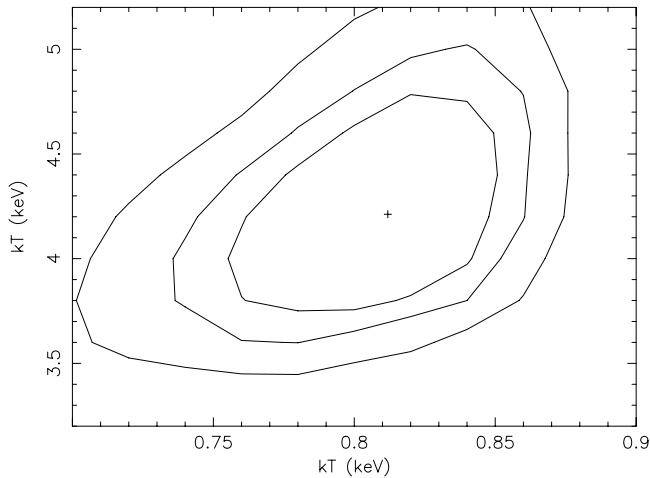
Fig. 9.—Contours on the fitted continuum parameters using the dual Raymond-Smith model applied to the PSPC + SIS data.

test their effects. For an abundance of 0.1 solar, the component temperatures lie well within the errors of the original fit. No abundance peculiarities were detected in the optical spectrum either, although the strength of the [N II] $\lambda6584$ line relative to Hα was considerably stronger in MF 16 than in any other SNR in NGC 6946 and indicates possible enrichment of nitrogen (BFS00).

As an aid to interpreting the observed X-ray data on MF 16, we used *HST* optical images (BFS00), which provide a wide-field view of the region. Within a square $\sim30''$ region with its eastern edge fixed on MF 16, potential X-ray contributors include the SNR MF 15 ($\sim15''$ to the northwest), an apparent OB association ($\sim10''$ to the west), a possible X-ray binary (XRB, $30''$ to the southwest), and MF 16 itself. SNR MF 15 is about an order of magnitude less bright than MF 16 in the optical and may be similarly faint in the X-ray. Also, because the OB association shows no evidence of abnormal brightness in the *HST* image, we assume its X-ray emission is the product of the emission from an average OB star and the number of member stars; that product is $\sim10^{34}$–10^{36} ergs s^{-1} (e.g., Gagné & Caillault 1994), well below the luminosity of MF 16. The possible XRB undoubtedly contaminates the spectrum, particularly at high energies, but with a luminosity ratio of ~15:1, the spectrum will not be dominated by the XRB's emission below ~3 keV.

Determining the precise physical locations of the observed X-rays coming from MF 16 is not possible from the present low spatial resolution data sets. However, several sources are likely: each of the SNR shells or the optically bright, crescent-shaped interaction region where two of the SNRs are apparently colliding (BFS00). Each source's emission, unfortunately, cannot be uniquely deconvolved from the observed spectrum and two equally valid models fit the MF 16 spectrum: a power-law continuum plus emission-line or dual thermal components consisting of bremsstrahlung or Raymond-Smith spectra. The plausibility of a thermal model is questionable on the grounds of a lack of thermal line emission yet appears more physically likely given that other SNRs possess thermal components with temperatures of ~0.2 keV (e.g., the Cygnus Loop, Miyata et al. 1994). Therefore, in the following discussion, we adopt the dual Raymond-Smith model.

If we treat the interaction of the two shocks as approximately equivalent to a shock impacting a wall (as in the Cygnus Loop—Levenson et al. 1997; Hester, Raymond, & Blair 1994), then the cooler component of the *ASCA* spectrum should describe the summed emission of both SNRs, leaving the hard spectral component to describe the interaction region. This component assignment has a precedent. Simulations (e.g., Pittard & Stevens 1997) and *ASCA* observations (Maeda et al. 1999) of colliding winds in O-star binaries show the harder component (~2–3 keV) is emitted by the interaction region. The emission measure (EM $\sim n^2V$, for density n and volume V) is directly related to the normalization of the Raymond-Smith component. Assuming two spherical SNRs of diameters of ~8 and ~20 pc (BFS00) each contributing half the total, we estimate electron densities of ~35 and ~10 cm^{-3}, respectively, in good agreement with the preshock density values inferred from the postshock, optical [S II] $\lambda\lambda6716$, 6731 line ratio (BFS00).

For the optically bright interaction crescent region, we estimate an upper limit to the electron density assuming that the hard spectral component is not strongly contaminated by emission from other nearby sources. Model simulations of colliding SNRs show such interactions will generate a ringlike contact zone that then expands outward as the shells merge (e.g., Ikeuchi 1978; Voinovich & Chernin 1995). Assuming the interaction region is also a torus, the fitted emission measure and the toroid volume yield a density of ~100 cm^{-3}. Contamination of the hard component will lower this estimate. At the interface, we expect the thermal and ram pressures of each SNR to be approximately equal. Since the density ratio is ~3–4, the shock velocity ratio must be ~1.7–2. Spatially resolved X-ray spectroscopy will provide valuable constraints on the relative strengths of the two shocks.

Models of colliding SNRs assume a homogeneous circumprogenitor medium (Ikeuchi 1978; Voinovich & Chernin 1995). If such a medium described the MF 16 region, the SNRs would eventually merge to one remnant (e.g., Ikeuchi 1978). However, we have uncovered evidence for an inhomogeneous medium. Furthermore, the *HST* data suggest the possibility of a cavity explosion (BFS00), further complicating the dynamics and clouding our understanding of the origin and evolution of the SNR complex. Given the already high optical, radio, and X-ray luminosity of this remarkable SNR complex, such a merger could be related to especially large, energetic SNRs (hypernovae remnants) recently identified in other galaxies (M101; Wang 1999). In any case, further study of this extraordinarily luminous X-ray region should help shed new insights on the properties of SNR shock emission under high-density situations.

4. SUMMARY

We have presented the data from an *ASCA* and a *ROSAT* HRI observation of the spiral galaxy NGC 6946. The *ASCA* image represents the first look at this galaxy above 2 keV. The *ASCA* image contains evidence for diffuse emission in the inner $\sim4'$ extending to energies greater than 2 keV. Fourteen pointlike sources are detected in the HRI observation. One source corresponds to the very luminous SNR complex uncovered in the PSPC data. The HRI resolves a point source $\sim30''$ west of the SNR complex that could not be detected in the PSPC data. The luminosity of

the point source is ∼1/15 of the SNR complex. None of the point sources shows evidence of variability.

Two possible spectral fits to the *ASCA* spectrum of the SNR complex provide contrasting interpretations. The spectrum can be fitted either by a power-law plus an emission-line or by dual Raymond-Smith thermal plasma models with differing temperatures. We argue that the dual thermal models provide a physically plausible interpretation.

REFERENCES

Blair, W. P., & Fesen, R. A. 1994, ApJ, 422, L103
Blair, W. P., Fesen, R. A., & Schlegel, E. M. 2000, AJ, in press (BFS00)
Briel, U., et al. 1996, *ROSAT* Users' Handbook
Burstein, D., & Heiles, C. 1984, ApJS, 54, 33
Colbert, E. J. M., & Mushotzky, R. F. 1999, ApJ, 519, 89
David, L., Harnden, F., Jr., Kearns, K., & Zombeck, M. 1995, High Resolution Imager Calibration Report
de Vaucouleurs, G. 1979, ApJ, 227, 729
Dotani, T., Yamashita, A., Ezuka, H., Takahashi, K., Crew, G., Mukai, K., & the SIS Team. 1997, *ASCA* Newsl. 5
Dunne, B. C., Gruendl, R. A., & Chu, Y.-H. 2000, AJ, 119, 1172
Fabbiano, G. 1994, in X-Ray Binaries, ed. W. Lewin, J. van Paradijs, & E. van den Heuvel (Cambridge: Cambridge Univ. Press), 390
Fabbiano, G., & Trinchieri, G. 1987, ApJ, 315, 46
Gagné, M., & Caillault, J.-P. 1994, ApJ, 437, 361
Hester, J. J., Raymond, J., & Blair, W. 1994, ApJ, 420, 721
Ikeuchi, S. 1978, PASJ, 30, 563
Jalota, L., Gotthelf, E., & Zoonematkermani, S. 1993, Proc. SPIE, 1945, 453
Kallman, T., Liedahl, D., Osterheld, A., Goldstein, W., & Kahn, S. 1996, ApJ, 465, 994
Kim, S.-W., & Chun, M.-S. 1984, J. Korean Astron. Soc., 17, 23
Kormendy, J., & Richstone, D. 1995, ARA&A, 33, 581
Krautter, J., et al. 1999, A&A, 350, 743
Kürster, M., & Hasinger, G. 1993, Internal MPE Memo, March 10
Lacey, C., Duric, N., & Goss, W. 1997, ApJS, 109, 417
Levenson, N. A., et al. 1997, ApJ, 484, 304
Lorenz, H., Richter, G. M., Capaccioli, M., & Longo, G. 1993, A&A, 277, 321
Matonick, D. M., & Fesen, R. A. 1997, ApJS, 112, 49
Maeda, Y., Koyama, K., Yokogawa, J., & Skinner, S. 1999, ApJ, 510, 967

Micela, G., Sciortino, S., Kashyap, V., Harnden, F. R., Jr., & Rosner, R. 1996, ApJS, 102, 75
Miyata, E., Tsunemi, H., Pisarski, R., & Kissel, S. 1994, PASJ, 46, 101
Pfeffermann, E., et al. 1986, Proc. SPIE, 733, 519
Pittard, J., & Stevens, I. 1997, MNRAS, 292, 298
Predehl, P., & Schmitt, J. H. M. M. 1995, A&A, 293, 889
Prestwich, A., et al. 1997, presented at the Estes Park (CO) High Energy Astrophysics Division meeting, November
Schlegel, D. J., Finkbeiner, D., & Davis, M. 1998, ApJ, 500, 525
Schlegel, E. M. 1994a, ApJ, 434, 523
———. 1994b, ApJ, 422, L99
Schlegel, E. M., Petre, R., & Colbert, E. 1996, ApJ, 456, 187
Schlegel, E. M., Petre, R., Colbert, E., & Miller, S. 2000, in preparation
Simien, F., & de Vaucouleurs, G. 1986, ApJ, 302, 564
Snowden, S. 1995, Cookbook for Analyzing *ROSAT* Observations of Extended Objects and Diffuse Emission, US *ROSAT* Science Data Center (Greenbelt: NASA-GSFC)
———. 1998, ApJS, 117, 233
Snowden, S., Plucinsky, P., Briel, U., Hasinger, G., & Pfeffermann, E. 1992, ApJ, 393, 819
Tanaka, Y., Inoue, H., & Holt, S. 1994, PASJ, 46, L37
Van Dyk, S. D., Sramek, R. A., Weiler, K. W., Hyman, S. D., & Virden, R. E. 1994, ApJ, 425, L77
Voinovich, P. A., & Chernin, A. D. 1995, Astron. Lett., 21, 835
Wang, Q. 1999, ApJ, 517, 27
White, N., Nagase, F., & Parmar, A. 1995, in X-Ray Binaries, ed. W. Lewin (Cambridge: Cambridge Univ. Press), 1
Williams, R. M., Chu, Y.-H., Dickel, J. R., Beyer, R., Petre, R., Smith, R. C., & Milne, D. K. 1997, ApJ, 480, 618
Zimmermann, H.-U., et al. 1994, Nature, 367, 621